Journal of Catalysis 284 (2011) 60–67

Contents lists available at SciVerse ScienceDirect

Journal of Catalysis

journal homepage: www.elsevier.com/locate/jcat

High performance vanadia–anatase nanoparticle catalysts for the Selective Catalytic Reduction of NO by ammonia

Steffen B. Kristensen [a], Andreas J. Kunov-Kruse [a], Anders Riisager [a], Søren B. Rasmussen [b], Rasmus Fehrmann [a,*]

[a] Department of Chemistry and Centre for Catalysis and Sustainable Chemistry, Building 207, Technical University of Denmark, DK-2800 Kgs. Lyngby, Denmark
[b] Instituto de Catálisis y Petroleoquimica, Consejo Superior de Investigaciones Cientificas, Marie Curie 2, Campus de UAM, 28020 Madrid, Spain

ARTICLE INFO

Article history:
Received 14 February 2011
Revised 26 August 2011
Accepted 31 August 2011
Available online 5 October 2011

Keywords:
$deNO_X$
Selective Catalytic Reduction (SCR)
NO
Ammonia
Vanadia–anatase nanoparticles
Potassium resistivity

ABSTRACT

Highly active nanoparticle SCR $deNO_X$ catalysts composed of amorphous vanadia on crystalline anatase have been prepared by a sol–gel, co-precipitation method using decomposable crystallization seeds. The catalysts were characterized by means of XRPD, TEM/SEM, FT-IR, nitrogen physisorption and NH_3-TPD. Due to the high-surface area anatase particles, loading of 20 wt% vanadia could be obtained without exceeding monolayer coverage of V_2O_5. This resulted in unprecedented high $deNO_X$ SCR activity corresponding to a factor of two compared to an industrial reference and to other V_2O_5/TiO_2 catalysts reported in the literature in the examined temperature range of 200–400 °C. The catalysts showed very high resistivity towards potassium poisoning maintaining a 15–30 times higher activity than the equally poisoned industrial reference catalyst, upon impregnation by 280 μmole potassium/g of catalyst.

1. Introduction

The catalytic cleaning of flue gases for nitrogen oxides (NO_X) in stationary industrial sources, like power plants, is most often done using V_2O_5/TiO_2-based SCR (Selective Catalytic Reduction) catalysts (promoted by WO_3 or MoO_3) which reduce NO_X to nitrogen and water by injected ammonia. The efficiency of state-of-the-art catalysts is high when applied to flue gases from fossil fuels like oil and coal. However, the use of biomass (straw, wood) alone or as co-fuel is of increasing importance because this type of fuel is considered CO_2 neutral. Unfortunately, the flue gas becomes very poisonous towards the V_2O_5/TiO_2 catalyst due to increased content of alkaline potassium salts (i.e., KCl, K_2SO_4 and K_2O) originating from the biomass combustion. These salts, as particles or aerosols, are considered to eliminate Brønsted acid sites on vanadium (V—OH) by substituting the protons of OH-groups with potassium ions forming V—O—K groups [1–4]. Since the Brønsted acid sites are essential for the activation of ammonia [5], the catalyst deactivates rapidly in biomass flue gases, demanding replacement and/or cleaning of the catalyst within intervals of less than 2000 h on stream [6]. This procedure requires inconvenient and expensive shut down of the power plant.

In the present work, we have focused on improving the activity of the traditional V_2O_5/TiO_2 SCR catalyst as a way to prolong the time on stream where the catalyst retains sufficiently high activity.

The activity of the industrial V_2O_5/TiO_2-based SCR catalyst is limited by the surface area and acidity of the anatase carrier. Since only up to one monolayer of the vanadium oxide species, i.e., a theoretical maximum of 7–8 Vanadium atoms/nm^2 [7,8], shows high activity and selectivity, commercial catalysts only accommodate a vanadia loading of 3–5 wt% due to the low surface area of the support. Exceeding the monolayer capacity of the carrier with a high vanadia loading leads to formation of crystalline V_2O_5, which exhibits decreased $deNO_X$ activity and increased ability to oxidize NH_3 and possibly also SO_2 in the flue gas [9]. One approach to improve the efficiency of catalytic materials is to prepare them as very small nanosized particles. Smaller particles have an increased surface area compared with the same mass of larger particles, which allows them to accommodate more of the catalytic active monolayer. Hence, it is very likely that a catalyst based on tiny nanocrystals of TiO_2 with a monolayer of amorphous V_2O_5 will be able to reduce NO_X with increased efficiency and lifetime in biomass fired applications, thus complying with demand for sufficient activity during prolonged operation.

Another parameter that limits activity in traditional V_2O_5/TiO_2 SCR catalysts and further makes them very sensitive to alkali poisoning is the relatively poor acidic properties of anatase. Pure

* Corresponding author. Fax: +45 45883136.
E-mail address: rf@kemi.dtu.dk (R. Fehrmann).

0021-9517/$ - see front matter © 2011 Elsevier Inc. All rights reserved.
doi:10.1016/j.jcat.2011.08.017

anatase has only moderate acidity (H_0 = +1.5 on the Hammett acid scale [10]), whereas sulphated anatase prepared from sulphated amorphous TiO_2 exhibits super acidity ($H_0 > -11.93$ [10]). Introduction of additional strong acidic sites through sulphation promotes the overall catalyst activity by increasing the amount of adsorbed, activated ammonia. Even more importantly, the acidic sites can host the alkali ions during operation avoiding elimination of the active vanadia sites. Furthermore, sulphation of the carrier prior to calcination can stabilize small nanocrystals when formed and increase the specific surface area significantly [11].

The use of promoters such as Ce to increase the acidity of the catalyst is also a solution [12]. Another solution to the problem could be the use of alternative transition metal-based catalysts and support materials for SCR deNO_X catalysis, which are less sensitive to the presence of alkali salts in the flue gas [13–15]. This approach is currently under investigation.

In this work, vanadia–anatase catalysts with a narrow nanosize distribution and high-surface area were synthesized by a modified novel sol–gel procedure [16–18]. Involving concomitant hydrolysis of titanium(IV) and vanadium(V) alkoxides in the presence of ammonium salt crystallization seeds followed by sulphation with sulphuric acid [19]. The prepared materials were characterized by X-ray Powder Diffraction (XRPD), Transmission and Scanning Electron Microscopy (TEM and SEM), Fourier-Transform Infrared Spectroscopy (FT-IR), Temperature Programmed Desorption of Ammonia (TPD) and nitrogen sorption methods (BET). The resulting V_2O_5/TiO_2 catalysts with vanadia loading in the range 5–25 wt% were tested for SCR deNO_X activity and compared to an industrial state-of-the-art reference catalyst. Analogous vanadia/TiO_2 materials have also been previously prepared by flame synthesis [20,21], hydrothermal methods [22,23] and mechanical blending [24] and the former evaluated for SCR deNO_X. Notably, none of these catalysts have shown the same promising properties as the catalysts reported in this work.

2. Experimental

2.1. Catalyst preparation

Nanoparticular vanadia/anatase catalysts were prepared by hydrolysis of an acetous ethanol solution, containing titanium(IV) isopropoxide (97%, Lancaster) and vanadium(V) oxytriethoxide (95%, Aldrich), with an aqueous solution of ammonium nitrate (99.0%, Aldrich) forming solid seed crystals. In a typical preparation the $Ti(OC_3H_7)_4$, $VO(OC_2H_5)_3$ and acetic acid mixture was first diluted in absolute ethanol and then cooled to 0 °C in an ice bath. The aqueous ammonium nitrate solution was then added dropwise to the ethanolic solution under magnetic stirring to form a sol–gel. The molar ratio of the reactants was adjusted to Ti/V/acetic acid/water/ethanol/ammonium salt = 1:x:2:15:30:2, where x was varied according to the desired amount of vanadium required to obtain catalysts with vanadia loading between 5 and 25 wt%. Subsequently, the sol–gel was aged at room temperature for 48 h under stirring. In some cases, sulphuric acid was added to sulphate the titania and simultaneously remove acetic acid by esterification. Next, excess ethanol, water, acetic acid and liberated isopropanol were removed under reduced pressure (12 mbar, 70 °C). Finally, the remaining powder was calcined at 380 °C in an air stream (300 mL min^{-1}) to decompose the ammonium template and convert amorphous titania into crystalline anatase [19]. The calcination temperature was chosen to match normal maximum operating temperature of the SCR unit in a power plant. Potassium doping of catalysts was done by incipient wetness impregnation using an aqueous solution of KNO_3 (99%, Riedel-de Haën), followed by drying (100 °C) and dehydration at 250 °C to ensure formation of K_2O. All poisoned samples were impregnated with 280 μmole of potassium/g catalyst.

2.2. Catalyst characterization

BET surface areas of samples were determined by physical adsorption of nitrogen using a Micromeritics ASAP 2020 analyzer. XRPD diffractograms were obtained by collecting data for 60 min with a Huber Guinier G670 camera at 25 °C using Cu Kα radiation. FT-IR spectra were recorded using wafers comprising 1 mg of sample mixed with 100 mg KBr using a Perkin-Elmer 1710 Infrared Fourier-Transform Spectrophotometer. The spectra were measured under ambient conditions using 30 scans. TEM micrographs were obtained using a Titan Analytical 300 kV transmission electron microscope, and SEM images were recorded using an Inspect 'S' scanning electron microscope with a tungsten filament electron source. The ammonia temperature programmed desorption was performed on a Micromeritics Autochem II Chemisorption analyzer with TCD detector. The samples were outgassed at 100 °C for 1 h in helium (99.999%, AGA), saturated with ammonia in a 50 mL min^{-1} flow of 1% NH_3 in He (AGA) and flushed with helium for 1 h, and finally, the TPD experiment was performed with a heating rate of 10 °C min^{-1}. Influence of desorbed SO_2 from the sulphated samples on the TPD profiles was eliminated by carrying out a NH_3-TPD experiment using He instead of NH_3.

2.3. Catalytic activity tests

Prior to the activity measurements, powdered samples were made into pellets (pressurized by 2.5 kbar), which were crushed and sieved to obtain particle fractions of 0.150–0.300 mm. SCR activity measurements were performed in a fixed-bed reactor using 8 mg catalyst diluted in 142 mg of SiO_2 (Quartz, Merck) with the same particle size. The mixture was loaded between the two layers of quartz wool in a quartz tube with an inner diameter of 5 mm. These conditions ensured isothermal plug-flow conditions, as previously described [25]. The reactant gas composition used in all the activity tests was 1000 ppm NO, 1100 ppm NH_3, 3% O_2 and balance He obtained from mixing of 1 vol% NO in He (±0.05% abs.), 1 vol% NH_3 in He (±0.05% abs.), O_2 ($\geqslant$99.95%) and helium (99.999%) (all from AGA) with a total flow rate of 700 mL min^{-1}. These conditions resulted in a gas hourly space velocity of 1,240,000 h^{-1} calculated from the volume of the active catalyst particles. The SCR reaction is known to be first order with respect to NO on vanadia catalysts under stoichiometric NH_3 conditions [26,27]. By assuming plug-flow conditions in the reactor, the performance can be expressed as the apparent first-order rate constant: $k = -F_0 \cdot [NO]_0^{-1} \cdot m_{cat}^{-1} \cdot \ln(1 - X)$, were F_0 is the molar NO feed rate, $[NO]_0$ the molar NO concentration at the inlet, X the NO conversion fraction and m_{cat} the mass of the catalyst [28]. The use of first-order rate constants as a measure of catalytic activity allows a direct comparison with other studies using different experimental conditions, e.g., catalyst masses and gas flows. NO and ammonia concentrations were measured at steady-state gas outlet concentrations with NO conversions $\leqslant$75% by online UV–VIS spectrophotometry using a Perkin Elmer Lambda 11 spectrometer (10 cm gas cell). SO_2 oxidation tests were performed with 80 mg catalyst exposed to 2000 ppm SO_2, 4.5% O_2 and He as balance ensuring a flow rate of 400 mL min^{-1}. Exposure time were 7200 min at 340–420 °C. Oxidized SO_2 was collected in a absorption column heated to 80 °C. Formed SO_3 were collected by a 20 wt% aqueous in isopropanol solution, and the amount of SO_3 was determined by titration with $Ba(ClO_4)_2$ using Thorin indicator.

3. Results and discussion

3.1. X-Ray powder diffraction

XRPD analysis of previously prepared, nanoparticular vanadia–titania catalysts using NH_4Cl as a crystallization seed [18] revealed only crystalline anatase as support phase with no peaks originating from residual crystalline NH_4Cl or V_2O_5. However, the samples did show a new phase suggesting either a crystalline vanadium-titania phase or a vanadium chloride phase. Catalysts in this work prepared with NH_4NO_3 as crystallization seed even with amounts of vanadia surpassing the monolayer limit of 8 V atoms/nm^2 showed likewise no crystalline V_2O_5. This indicates a high dispersion of an amorphous vanadia phase as typically found for oxide-supported vanadia catalysts [7,8]. However, the samples did contain a new phase originating from either a crystalline vanadia–titania phase or a more likely brookelite phase. This was observed only for unsulphated catalysts confirming that the H_2SO_4 acts as a crystal structure directing agent, which has been concluded before [29].

However, the vanadia–titania catalysts prepared in this work using NH_4NO_3 as the crystallization seed did not show the unidentified phase (see Fig. 1). This supports the vanadia–chloride phase hypothesis proposed in previous work [18] when using NH_4Cl as seed crystal. Hence, vanadium appeared to be dispersed on the surface of small anatase crystallites as amorphous vanadia–chloride or as pure vanadia depending on the selected crystallization seed. In accordance with this, no shifts of XRD reflections were observed, indicating no incorporation of vanadia into the anatase framework.

The size of the oxide crystallites formed was calculated by Scherrer's equation (using the peak at angle $2\theta = 25.3°$) to be in the range 7–15 nm, with no direct correlation with the vanadia content (see Table 2). But sulphation of catalysts as a last step in the preparation procedure before drying decreased the crystallite size, as shown in Table 2. Sequential measurements of the samples during calcination revealed that anatase crystallization was initiated around 300 °C followed by crystal growth until the particles reached the reported equilibrium size after 4 h. BET measurements (Table 2) of the catalysts revealed a correlation between increased vanadia loading and increased surface area. This could be explained by formation of amorphous V_2O_5 "islands" on the surface, which decreases the surface smoothness but increases the surface area. BET surface areas were also found to increase approx. 20 m^2/g upon sulphation, compared to the analogous non-sulphated catalysts.

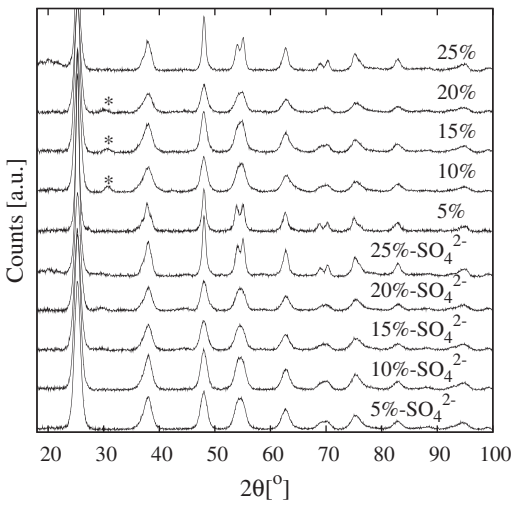

Fig. 1. Selected powder diffractograms of prepared vanadia–titania catalysts, with numbers indicating wt% V_2O_5 and SO_4^{2-} sulphated catalysts. All reflections indicate anatase crystal structure except reflections indicated with ∗, which originate from the brookelite crystal form.

3.2. TEM and SEM

TEM images of the 15 wt% vanadia–titania catalysts synthesized with sulphuric acid confirmed the high degree of crystallinity of the anatase support (Fig. 2). The crystal sizes were estimated by size measurement of 70 crystals, and the results agreed well with the XRPD results. The sample also exhibited a very narrow crystal size distribution ranging from 4 to 9 nm with a mean size of 6 nm. No evidence of crystalline V_2O_5 was found despite the fact that crystallization is well known to occur in heavily loaded catalysts [30]. This indicates that the nanoparticle-based catalysts can accommodate much more vanadium than conventional catalysts without forming crystalline vanadia.

A single crystal from the sample was investigated by Fast Fourier-Transformation (FFT) to determine the crystal planes and thereby the crystal type. The FFT showed that the interplanar spacing of the (101) and ($\bar{1}$01) planes were 3.5 Å and that the intersecting angle of the planes was 124°. The (004) interplanar spacing was measured to be 2.4 Å, and the angle between plane (101) and (104) was 27°. These results were identical to previous results obtained by XRPD and TEM on anatase in the literature [31,32]. SEM investigations confirmed nanocrystal agglomerates, but these particles showed a high degree of porosity, hence the maintained high-surface area.

3.3. Fourier-Transform Infrared Spectroscopy

The V=O stretch in crystalline V_2O_5 gives rise to a sharp and intense band at 1020 cm^{-1} [7,8]. When V_2O_5 is bound to anatase, the V=O band is weakened and the IR signal shifts to a broad band at 980 cm^{-1} [7,8] and is thus easily distinguished from the crystalline V_2O_5 phase. The recorded IR spectra of selected catalysts (Fig. 3) revealed a shoulder or a broad band at around 970 cm^{-1} due to the V=O stretch, while no peak at 1020 cm^{-1} was found in any of the spectra. The shift of the band, i.e., weakening of the V=O band, indicated a stronger interaction between VO_x species and the anatase [7,8].

Broadening of the band around 970 cm^{-1} was observed at loadings of 25 wt.% V_2O_5. Though the amorphous and strongly bonded V_2O_5 phase was still dominant, the broadening towards higher wave numbers indicated other species with a slightly increased V=O band strength originating from amorphous V_2O_5 phases with weaker or no bonding to the anatase surface. Thus, even far above the monolayer capacity of 8 vanadium atoms/nm^2, no presence of crystalline vanadia was indicated by TEM, XRPD or FT-IR. This further suggests that the new concomitant seed-assisted hydrolysis of titanium(IV)isopropoxide and vanadium(V)oxoethoxide results in a much more dispersed vanadia phase than is normally observed with more traditional impregnation methods. Several models for the formation of acidic sites due to sulphate species have been proposed [33,34], and it is well known that sulphating of anatase induces both Brønsted and Lewis sites of medium to strong acid strength [10]. The FT-IR spectra of catalysts with H_2SO_4 added before drying and calcination showed several new peaks at 1215, 1135 and 1043 cm^{-1}. These are all characteristic vibrations from monomeric sulphate species bound bidentately to anatase [34–37]. A sharp band at 1380 cm^{-1} associated with anhydrous sulphates is normally reported in the literature for sulphated TiO_2 [34,35]. In the present samples, this band was absent most probably due to hydration of the species, which is known to occur at lower temperatures and under humid conditions [34]. Furthermore, the weak peak at 1405 cm^{-1} could originate from small amounts of pyrosulphate dimers [38]. Though, it was more likely to originate

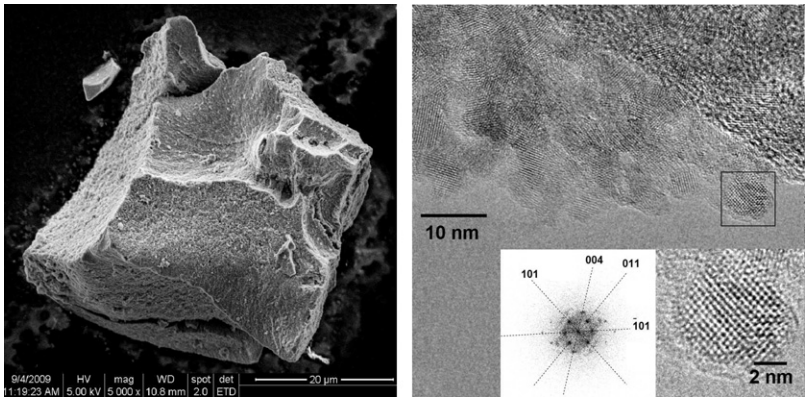

Fig. 2. TEM micrograph of 15 wt% V_2O_5/TiO_2 single crystal, zoom (framed area) and FFT of this area (right). SEM micrograph of a particle from the same sample (left).

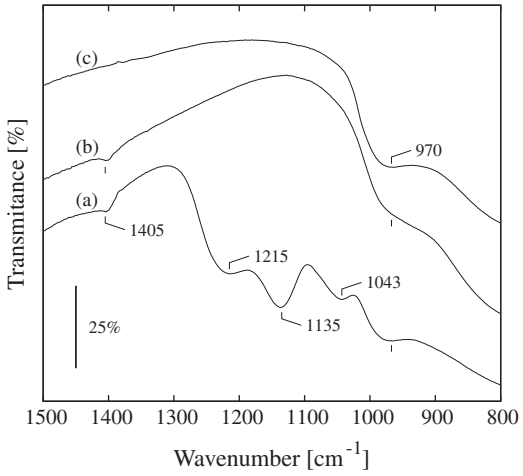

Fig. 3. Transmission FT-IR spectra of 1 mg catalyst in 100 mg KBr at ambient conditions. (a) 15 wt% V_2O_5/SO_4^{2-}—TiO_2, (b) 15 wt% V_2O_5/TiO_2, (c) 25 wt% V_2O_5/TiO_2.

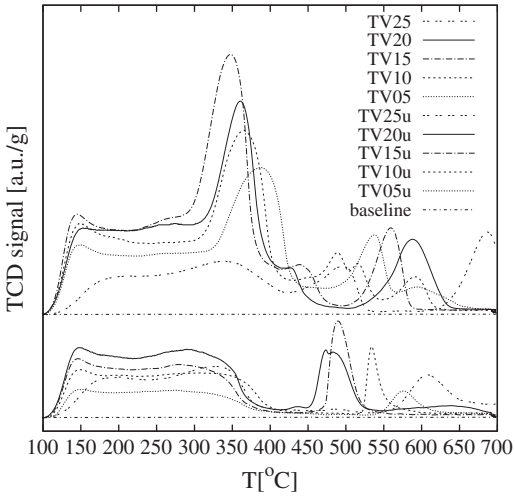

Fig. 4. NH_3-TPD profiles of catalysts. Baseline measured without saturation with NH_3 of a 15 wt% V_2O_5/SO_4^{2-}—TiO_2 catalyst, TV05-25: Sulphated 5–25 wt%V_2O_5/TiO_2 catalysts, TV05-25 u: Unsulphated 5–25 wt% a V_2O_5/TiO_2 catalysts.

from traces of ammonium ions [29] since it was found in both sulphated and unsulphated samples. For metal oxide-supported sulphates, it is well known that Brønsted acidity is more dominant at lower temperatures and humid conditions whereas Lewis acidity is more dominant at higher temperatures and dry conditions [10]. Due to this fact, no further attempts have been made currently to characterize the type of acidic surface sites, because all spectra were recorded under ambient conditions. However, a more thorough spectroscopic investigation of the catalytic surface sites will be presented in future work.

3.4. Temperature programmed desorption

NH_3-TPD profiles of the catalysts, the calculated corresponding total adsorbed ammonia and the specific acidities are illustrated in Fig. 4 and Table 1, respectively. The specific acidity was, as expected for the unsulphated catalysts, very similar to the industrial reference catalyst, although the strength of the acidic sites in the reference catalyst seemed to be slightly weaker. The total amount of acidic sites in all the nanoparticle catalysts was higher due to the higher surface areas and V_2O_5 content.

By sulphation of the carrier, a significant increase in the amount of acidic sites of varying strength was observed corresponding to a total acidity of up to three times that of the unsulphated samples. A background was also performed to exclude decomposition products originating from adsorbed sulphate. A peak at around 380 °C in the TPD profile indicated that the sulphation of the carrier induced sites with relatively high acid strength. These stronger sites are expected to be crucial to the SCR activity of the catalysts, as weaker acidic sites will be unable to adsorb ammonia at the typical operating temperatures of around 350–400 °C. A small part of the

Table 1
Ammonia TPD of the catalysts.

V_2O_5 (wt%)	Desorbed ammonia[a] (cm^3/g)	Specific acidity[a] (NH_3/nm^2)
5[b]	38	7.3
10[b]	48	8.4
15[b]	55	8.9
20[b]	48	6.3
25[b]	24	4.1
5[c]	10	3.7
10[c]	18	3.5
15[c]	24	4.9
20[c]	30	4.7
25[c]	15	4.5
Ref.[d]	12	4.5

[a] The acidity was calculated only on the basis of acidic sites with intermediate strength (<500 °C) since higher and super acidic sites are not likely to take part in the SCR-reaction.
[b] Sulphated 5–25 wt% V_2O_5/TiO_2.
[c] Unsulphated 5–25 wt% V_2O_5/TiO_2.
[d] Industrial reference catalyst with 3 wt% V_2O_5-7 wt% WO_3 on TiO_2.

acidic sites generated on both sulphated an unsulphated catalysts seemed to be very strong with peak values as high as 500, 670 and 700 °C. These sites could be strongly acidic or even super acidic undercoordinated titanium atoms on the carrier surface, created by the strong inducing effect of the sulphate species, as suggested by both experimental [32,33,39] and quantum mechanics studies [40,41] of similar sulphated metal oxides. A strong Lewis acid is characterized by a strong polarizing power. This polarization of the ammonia molecule results in a strengthening of the N—H band. This is directly observed with FT-IR as an upward shift of the symmetric N—H bending wave number [42]. A crucial step for the SCR mechanism is the activation of ammonia, which can be either a complete or a partial transfer of hydrogen from ammonia to a redox centre [5,9,43–46]. Accordingly, it is considered doubtful that the ammonia adsorbed on the very acidic sites associated with the peaks 500, 670 and 700 °C in the TPD profile plays any significant role in the SCR reaction, as the activation of this ammonia would require breakage of a significantly stronger N—H bond compared to the majority of the ammonia species associated with desorption peaks around the catalyst's working temperature (350–400 °C). Therefore, these peaks are excluded in the calculations in Table 1. However, the strong acidic sites may still be able to host alkali compounds and thereby preserve activity in case of alkali poisoning.

Table 1 shows that the amount of desorbed ammonia increases with increasing V_2O_5 content until an optimum is reached at 15–20 wt%. The specific acidity, by contrast, follows no clear trend other than that sulphation increases the acidity. Indicating that sulphation increases the acidity whereas the V_2O_5 content has no direct influence on specific acidity, but total acidity increases due to the increase in surface area.

3.5. Catalytic activity measurements

Catalytic activity was measured at temperatures from 200 to 450 °C to find activity maxima. The prepared catalysts exhibited remarkable SCR activities, as illustrated in the plot of the measured rate constants *k* vs. temperature in Fig. 5 (catalysts synthesized without added sulphuric acid).

The optimum vanadium loading was observed at 20 wt% vanadia by comparing the activity maxima where a rate constant almost twice as high as the commercial reference catalyst was observed.

It should be noted that the commercial reference catalyst has been calcined at a somewhat higher temperature, i.e., around 450 °C, than the catalysts studied here. The increased sintering expected at increased temperature leads to agglomeration of the vanadium oxide species resulting in somewhat increased $deNO_x$ and SO_2 oxidation activity as observed previously for industrial catalysts [47]. However, we find it more useful to compare our results with this industrial catalyst employed at 380 °C, rather than a less active conventional V_2O_5/TiO_2-based catalyst prepared by impregnation of a TiO_2 carrier with ammonium metavanadate and calcined at 380 °C.

From Fig. 5 it is also clear that the maximum activity temperature was gradually shifted from higher temperatures (around 480 °C) to lower temperatures (around 380 °C) with increasing vanadium loading. Since the maximum activity is reached where the competitive oxidation of NH_3 becomes more pronounced, the NH_3 oxidation must increase with increasing vanadium content. This trend is also observed for more traditionally prepared catalysts, due to formation of more active, but less selective, polymeric vanadia species [9,48]. The activity increases even further through adding sulphuric acid to the sol–gel before drying and calcinations (Fig. 6), allowing a rate constant above 2000 $cm^3\ g^{-1}\ s^{-1}$ to be obtained. Comparing the catalysts at ideal SCR temperatures (350–380°) reveals the vanadium loading of choice to be 20 wt%, which is remarkably high compared to usual SCR catalyst loadings.

Working with nanoparticles always raises the question of sintering. Long-term stability tests of a 15 wt% V_2O_5/TiO_2 catalyst at 380 °C (industrial operational temperature) is in progress, however, a previous test of such catalyst doped with a small and probably insignificant amount of Au (1 wt%), indicated thermal stability for 500 h. Hysteresis was observed after heating to 460 °C possible due to sintering and evaporation of SO_4^2 acid sites, corresponding to an activity loss of 20% for the sulphated 20 wt% catalyst. This temperature is comparable with the calcination temperature for the industrial reference catalyst of 450 °C. Keeping the temperature below 420 °C only deactivated the catalyst 10%, and no deactivation was observed at 400 °C and temperatures below. A sulphated 15 wt% catalyst was calcined at 450 °C in air for 4 h in order to investigate possible reasons for the activity loss and hysteresis.

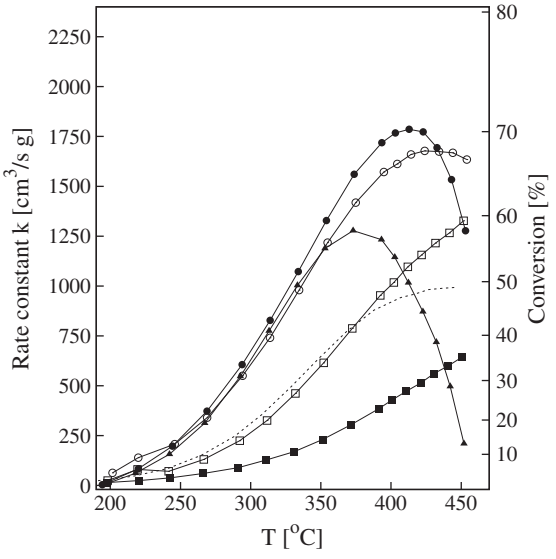

Fig. 5. Activity of unsulphated catalysts with varying V_2O_5 content: (■) 5 wt%, (□) 10 wt%, (○) 15 wt%, (●) 20 wt%, (▲) 25 wt%, (···) industrial reference 3 wt% V_2O_5 7 wt% WO_3 on TiO_2 catalyst.

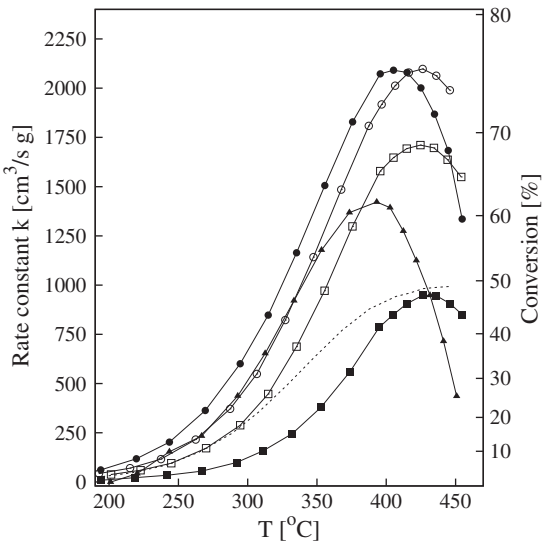

Fig. 6. Activity of sulfated catalysts with varying V_2O_5 content: (■) 5 wt%, (□) 10 wt%, (○) 15 wt%, (●) 20 wt%, (▲) 25 wt%, (···) industrial reference 3 wt% V_2O_5 7 wt% WO_3 on TiO_2 catalyst.

Table 2
Characteristics of the prepared vanadia–anatase catalysts.

V_2O_5 (wt%)	$k_{max}(T_{max})$ (cm^3/g s) (°C))	E_a (kJ/mol)	S_{BET} (m^2/g)	$d_{particle}$[a] (nm)	n_s[b] (V/nm^2)
5[c]	948 (426)	54	129	7.5	2.6
10[c]	1711 (424)	53	144	7.7	4.6
15[c]	2097 (426)	52	151	7.1	6.5
20[c]	2091 (405)	49	189	7.7	7.0
25[c]	1422 (393)	51	89	13.9	18.6
5[d]	644 (450)	44	67	15.6	4.9
10[d]	1327 (451)	53	126	8.1	5.3
15[d]	1677 (424)	44	121	8.8	8.2
20[d]	1772 (423)	46	156	8.0	8.2
25[d]	1277 (373)	50	82	14.9	20.2
Ref.[e]	993 (446)	52	68	29.6	2.9

[a] Calculated by Scherrer's equation [52] (using the peak angle $2\theta = 25.3°$).
[b] Surface density of vanadium atoms calculated as $n_s = m_{V_2O_5} \cdot 2 \cdot N_A \cdot (m_{cat} \cdot M_{V_2O_5} \cdot S_{BET} \times 10^{18})^{-1}$.
[c] Synthesized using the NH_4NO_3 template followed by sulphation with sulphuric acid.
[d] Synthesized using the NH_4NO_3 template without sulphation.
[e] Industrial reference catalyst with 3 wt% V_2O_5-7 wt% WO_3 on TiO_2.

XRPD of this sample showed as for all the other catalyst samples only peaks from anatase and no indication of crystalline V_2O_5. However, the average anatase crystal size increased from 7.1 nm obtained for the very same 15 wt% catalyst calcined at 380 °C for 4 h (Table 2) to 15.6 nm pointing to agglomeration of the carrier particles as cause for the activity loss and hysteresis observed when the catalyst is calcined above 400 °C. Unsulphated catalysts suffered only slight deactivation upon heating, indicating that the thermal deactivation of sulphated catalysts are almost entirely due to evaporation of acid sites.

The advantage of the nanoparticle catalysts was even more pronounced when comparing resistance towards potassium poisoning , as clearly illustrated in Figs. 7 and 8. The six catalysts were all impregnated with 280 μmole potassium per gram of catalyst. All the non-sulphated catalysts maintained a relatively high activity at 380 °C, with the exception of the catalyst with 5 wt% loading that showed approximately the same deactivation as the reference catalyst. The most alkaline-resistant unsulphated catalyst was obtained with 20 wt% V_2O_5, which had an activity of approx. 600 $cm^3\,g^{-1}\,s^{-1}$. This corresponds to an activity 15 times higher

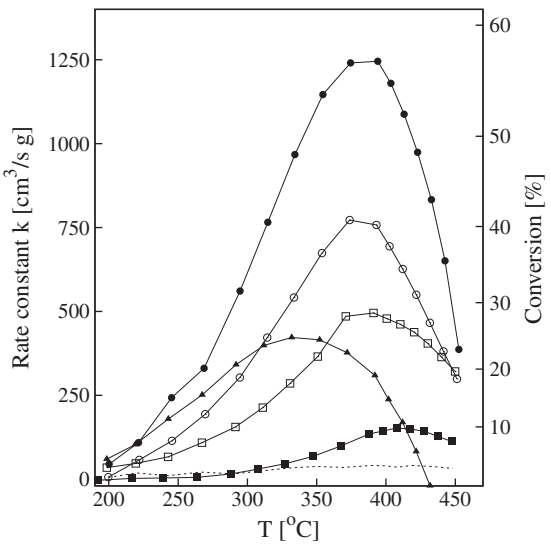

Fig. 7. Activity of potassium deactivated (280 μmole K /g) sulphated catalysts with varying V_2O_5 content: (■) 5 wt%, (□) 10 wt%, (○) 15 wt%, (●) 20 wt%, (▲) 25 wt%, (···) industrial reference 3 wt% V_2O_5 7 wt% WO_3 on TiO_2 catalyst.

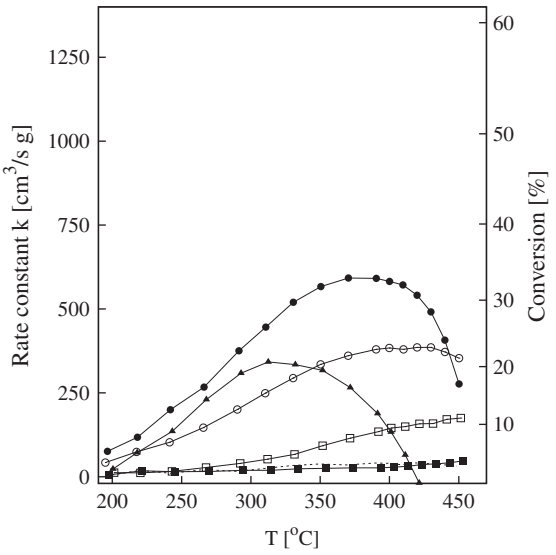

Fig. 8. Activity of potassium deactivated (280 μmole K/g) unsulphated catalysts with varying V_2O_5 content: (■) 5 wt%, (□) 10 wt%, (○) 15 wt%, (●) 20 wt%, (▲) 25 wt%, (···) industrial reference 3 wt% V_2O_5 7 wt% WO_3 on TiO_2 catalyst.

than the industrial reference catalyst at 380 °C. Upon sulphation, the resistance increased even more and the 20 wt% catalyst only deactivated by 40% resulting in an activity more than 30 times the potassium deactivated reference catalyst. All the catalysts revealed increased deactivation upon heating due to surface diffusion of potassium to the active sites above the K_2O Tamman temperature [49]. Furthermore, decomposition of formed sulphate-potassium species leads to liberation of potassium oxide as previously reported with sulphated catalysts [13].

3.6. Selectivity and stability

To investigate the activity at more realistic conditions, additional activity measurements were performed with H_2O and SO_2 in the flue gas, see Fig. 9. The first segment confirms the activity as previously illustrated at 380 °C in Fig. 6. In accordance with

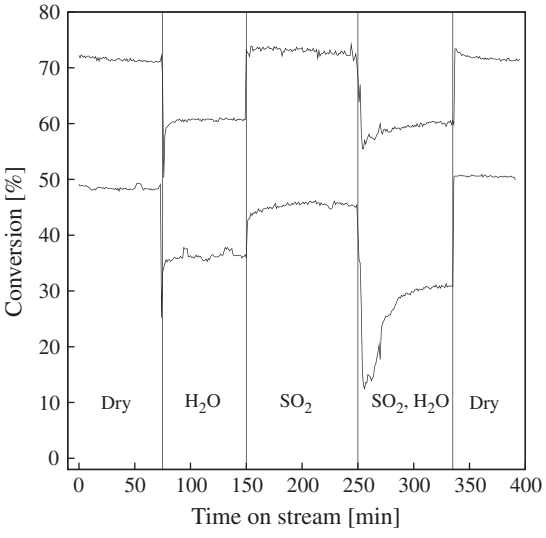

Fig. 9. Activity measurements of 20 wt% V_2O_5 sulphated and an industrial reference 3 wt% V_2O_5 7 wt% WO_3 on TiO_2 catalyst. Gas flow and composition 730 ml/min, dry: 1000 ppm NO, 1100 ppm NH_3, 3% O_2 and He balance, H_2O: additional 2.4% H_2O, SO_2: additional 2000 ppm SO_2 and H_2O, SO_2: the two combined.

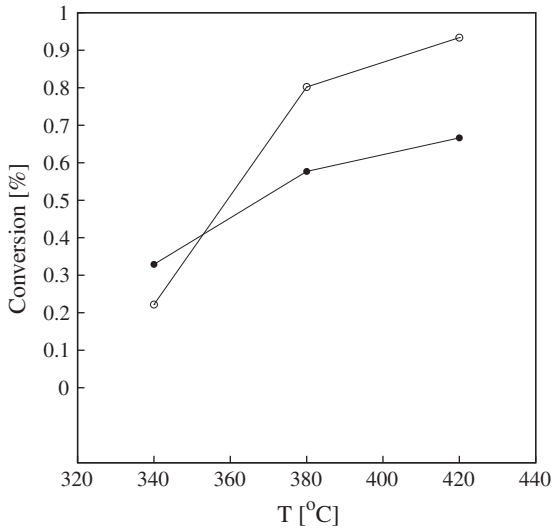

Fig. 10. SO_2 oxidation, (•) 20 wt% V_2O_5 sulphated, (○) the industrial reference 3 wt% V_2O_5 7 wt% WO_3 on TiO_2 catalyst. Gas flow composition 2000 ppm SO_2, 4.5% O_2 and He as carrier.

Turco et. al [50], the activity decreased in the presence of water, see second segment, where 2.4% H_2O is added and the activity decreased 10–12%. Introducing 2000 ppm of SO_2 and removing water increased the activity of the 20 wt% catalyst to conversions just above the initial. Activity of the industrial catalyst also increases in activity resulting in conversions just below the initial. By adding water, the activity decreased again by the same amount as before going from dry to wet gas, 10–12%. Last segment shows the initial activity again in dry flue gas demonstrating the high thermal and chemical stability of the 20 wt% V_2O_5 catalyst, displaying no activity loss due to H_2O or SO_2 treatment. SO_3 formation is a major concern due to fouling of the catalyst and heat exchangers downstream by NH_4HSO_4. Comparison of SO_2 oxidation between the industrial reference and the 20 wt% catalyst can be seen in Fig. 10. From this, it is clear that the 20 wt% V_2O_5 catalyst is exhibiting the same SO_2 oxidation properties as the industrial reference, despite the high V_2O_5 loading. Like wise selectivity measurements showed that the 15 wt% sulphated catalyst formed less N_2O in dry flue gas at 350–420 °C than the industrial reference catalyst, respectively, 13–62 and 33–146 ppm N_2O formed. But the formation vastly decreased in wet gas for both catalysts as expected from previous selectivity measurements in literature [51].

4. Conclusions

New types of highly active SCR deNO_X catalysts based on nanosized crystalline anatase has been synthesized. The synthesis method involved hydrolysis of titanium(IV) and vanadium(V) in ethanol solution with added acetic acid in the presence of a NH_4NO_3 crystallization template followed by sulphation with sulphuric acid. Different parameters in the synthesis protocol were investigated. XRPD and BET experiments revealed that NH_4NO_3 seeds gave smaller anatase crystals (6–8 nm) and larger surface areas (up to 189 m^2/g) than when using NH_4Cl in earlier studies [18]. Moreover, the use of NH_4NO_3 yielded samples of pure anatase without impurities from mixed phases (determined by XRPD and TEM). Sulphation with sulphuric acid increased the surface area, but more importantly it also increased the total acidity of the catalyst by a factor of approximately three and induced a significant increase in the strength of the acidic sites.

The optimal V_2O_5 content in the catalysts was found to be around 20 wt%, which is very close to one theoretical monolayer formed on the carrier surface. The surface species characterized by the V=O stretch with FT-IR showed a larger shift towards lower wave numbers than reported elsewhere in the literature, indicating a stronger bond between the anatase support and the active vanadia phase. When the theoretical monolayer was exceeded, no sign of crystalline V_2O_5 was detected by XRD, FT-IR or TEM, although the formation of weaker bonding species was indicated by FT-IR. Activity of the 20 wt% V_2O_5/SO_4^{2-}—TiO_2 catalyst had a maximum around 420 °C with the rate constant $k = 2100\ cm^3\ s^{-1}\ g^{-1}$, which is more than twice the value for the industrial state-of-the-art catalyst used as reference. The catalysts showed decrease in deNOx activity after heating to 420 °C and above. It is well known that the addition of tungsten oxide increases the thermal stability of industrial catalysts. Optimization of the thermal stability of the catalysts prepared here by addition of tungsten oxide will be the subject of studies in the near future. The new catalysts also demonstrated a large increase in resistance towards potassium poisoning. Thus, the deactivation by potassium poisoning of the commercial catalyst was 96% compared to only 64% and 40% for the 20 wt% V_2O_5–TiO_2 and 20 wt% V_2O_5/SO_4^{2-}—TiO_2 catalysts respectively at 380 °C. This means that the new catalysts maintained a 15-30 times higher activity than the industrial reference catalyst under SCR conditions after poisoning. These features make them highly attractive as promising SCR catalysts in power plants fired with CO_2 neutral biomass fuels.

Acknowledgement

Dong Energy A/S, Vattenfall A/S and Energinot.dk (FU3718) are thanked for financial support.

References

[1] J. Chen, R. Yang, J. Catal. 25 (2006) 411.
[2] H. Kamata, K. Takahashi, C.U.I. Odenbrand, J. Mol. Catal. A: Chem. 139 (1999) 189.
[3] I.E. Wachs, B.M. Weckhuysen, Appl. Catal. A 157 (1997) 67.
[4] D. Bulushev, F. Rainone, L. Kiwi-Minsker, Langmuir 17 (2001) 5276.
[5] N. Topsøe, H. Topsøe, J. Dumesic, J. Catal. 151 (1995) 226.
[6] P. Overgaard, K. Wieck-Hansen, O. Larsen, Biomass Bioenergy 19 (2000) 395.
[7] G. Busca, G. Centi, L. Marchetti, F. Trifiro, Langmuir 2 (1986) 568.
[8] G.C. Bond, S.F. Tahir, Appl. Catal. 71 (1991) 1.
[9] G. Busca, L. Lietti, G. Ramis, F. Berti, Appl. Catal. B 18 (1998) 1.
[10] J.R. Sohn, J. Ind. Eng. Chem. 10 (2004) 1.
[11] L. Baraket, A. Ghorbel, P. Grange, Appl. Catal. B 72 (2007) 37.
[12] L. Chen, J. Li, M. Ge, J. Phys. Chem. C 113 (2009) 21177.
[13] A. Kustov, M.Y. Kustov, R. Fehrmann, P. Simonsen, Appl. Catal. B 58 (2005) 97.
[14] A. Kustov, S. Rasmussen, R. Fehrmann, P. Simonsen, Appl. Catal. B 76 (2007) 9.
[15] J. Due-Hansen, S. Boghosian, A. Kustov, P. Fristrup, G. Tsilomelekis, K. Ståhl, C.H. Christensen, R. Fehrmann, J. Catal. 251 (2007) 459.
[16] Y. Hari-Bala, J. Zhao, Y. Jiang, X. Ding, Y. Tian, K. Yu, Z. Wang, Mater. Lett. 59 (2005) 1937.
[17] Y. Hari-Bala, J. Zhao, Y. Jiang, X. Ding, Y. Tian, K. Yu, Z. Wang, Mater. Lett. 60 (2006) 494.
[18] A. Kruse, S. Kristensen, A. Riisager, S. Rasmussen, R. Fehrmann, J. Mater. Sci. 44 (2009) 323.
[19] A. Kruse, S. Kristensen, A. Riisager, S. Rasmussen, R. Fehrmann, Patent Application 08169238.6-2104 (DTU), 2008.
[20] W. Stark, K. Wegner, S. Pratsinis, A. Baiker, J. Catal. 197 (2001) 182.
[21] B. Schimmoeller, H. Schulz, S. Pratsinis, A. Bareiss, A. Reitzmann, B. Kraushaar-Czarnetzki, J. Catal. 243 (2006) 82.
[22] L. Yu, X. Zhang, Chem. Phys. 87 (2004) 168.
[23] M. Mohamed, W. Bayoumy, M. Khairy, M. Mousa, Micropor. Mesopor. Mater. 97 (2006) 66.
[24] G. Liu, K. Wang, Z. Zhou, Mater. Sci. Forum 86 (2006) 510.
[25] C. Perego, S. Peratello, Catal. Today 52 (1999) 133.
[26] M. Inomata, A. Mlyamoto, T. Ui, K. Kobayashl, Y. Murakami, Ind. Eng. Chem. Prod. Res. Dev. 21 (1982) 424.
[27] H. Bosch, F. Janssen, Catal. Today 46 (1988) 217.
[28] R.Q. Long, R.T. Yang, J. Catal. 196 (2000) 73.
[29] M. Kanna, S. Wongnawa, Mater. Chem. Phys. 110 (2008) 166.
[30] D.A. Bulushev, L. Kiwi-Minsker, V.I. Zaikovskii, A. Renken, J. Mol. Catal. 193 (2000) 145.
[31] C. Su, B. Hong, C. Tseng, Catal. Today 96 (2004) 119.
[32] T. Akita, K. Tanaka, S. Tsubota, M. Haruta, J. Electron Microsc. 49 (2000) 657.
[33] J.R. Sohn, H.W. Kim, J. Catal. 101 (1986) 428.

[34] O. Saur, M. Bensitel, A.M. Saad, J.C. Lavalley, J. Catal. 99 (1986) 104.
[35] M. Waqif, J. Bachelier, O. Saur, J. Lavalley, J. Mol. Catal. 72 (1992) 127.
[36] S. Samantaray, P. Mohapatra, K.J. Parida, J. Mol. Catal. A 198 (2003) 277.
[37] J.R. Sohn, H.W. Kim, J. Mol. Catal. 52 (1989) 361.
[38] A. Desmartin-Chomel, J.L. Flores, A. Bourane, J.M. Cladens, F. Figueras, G. Delahay, J. Phys. Chem. B 110 (2006) 858.
[39] M. Hino, K. Arata, Mater. Chem. Phys. 26 (1990) 213.
[40] T. Kanougi, T. Atoguchi, S. Yao, J. Mol. Catal. A 177 (2002) 289.
[41] A. Hofmann, J. Sauer, J. Phys. Chem. B 108 (2004) 15679.
[42] G. Busca, Catal. Today 41 (1998) 191.
[43] M. Calatayud, C. Minot, J. Phys. Chem. B 108 (2004) 15679.
[44] A. Vittadini, M. Casarin, A. Selloni, J. Phys. Chem. B 109 (2005) 19560.
[45] S. Soyer, A. Uzun, S. Senkan, I. Onal, Catal. Today 118 (2006) 268.
[46] M. Anstrom, N. Topsøe, J. Dumesic, J. Catal. 213 (2003) 115.
[47] A. Forzatti, P. Nova, I. Beretta, Catal. Today 56 (2000) 431.
[48] G. Went, L. Leu, R.R. Rosin, A.T. Bell, J. Catal. 143 (1992) 492.
[49] D.R. Lide, Handbook of Chemistry and Physics, CRC, 2007.
[50] M. Turco, L. Lisi, R. Pirone, Appl. Catal. B 3 (1994) 133.
[51] N. Topsøe, T. Slabiak, B.S. Clausen, T.Z. Srnak, J.A. Dumesic, J. Catal. 134 (1992) 742.
[52] A.L. Patterson, Phys. Rev. 56 (1939) 978.